State-feedback control of grid and circulating current in modular multilevel converters

Antoneta Iuliana Bratcu, Remus Teodorescu

State-feedback control of grid and circulating current in modular multilevel converters

Antoneta Iuliana Bratcu*, Remus Teodorescu**

**Univ. Grenoble Alpes, CNRS, Grenoble INP[*], GIPSA-lab, 38402, Saint-Martin d'Hères Cedex, France*
[*]Institute of Engineering Univ. Grenoble Alpes (Tel: +33476826384; e-mail: antoneta.bratcu@gipsa-lab.grenoble-inp.fr).
***Department of Energy Technology, Aalborg University,*
Aalborg, Denmark, (e-mail: ret@et.aau.dk)

Abstract: This paper proposes a state-feedback control of both grid and circulating current in modular multilevel converters (MMCs), which ensures that the input-coupled dynamics of the two currents to be controlled within a multi-input–multi-output (MIMO) approach. A systematic design procedure is detailed and the strategy is validated on a comprehensive MATLAB®/Simulink® model of a three-phase MMC. Simulation results show that, compared with the conventional control featuring two separate control loops, the proposed control shows better performance under unbalanced grid conditions.

Keywords: application of power electronics, control system design, linear multivariable systems, disturbance rejection, filtering and smoothing.

1. INTRODUCTION

Voltage-source-converter (VSC)-based high-voltage DC (HVDC) transmission is an attractive technique for large offshore wind power plants (Sharifabadi *et al.*, 2016). In 2002, a new type of multilevel converter, the modular multilevel converter (MMC), was proposed (Marquardt *et al.*, 2002). It represents a shift in the power electronics converters technology, which consists in multiplying number of layers containing switching devices. Operation at a switching frequency lower than in previous topologies is thus possible. Lower losses and higher operating efficiency also are obtained. Due to its modularity, scalability, high efficiency and low harmonic distortion, in addition to all other merits of VSCs, MMC has earned increasing attention during these years, being the preferred solution in the field of high-voltage DC power transmission for offshore wind power plants.

Instead of a large DC-side capacitor, MMCs have many lower-capacity capacitors, behaving like a sort of spatially distributed energy storing capacity. The MMC as a plant is complex due to the high number of submodule capacitors (SM) and strongly nonlinear as output current and internal circulation current are coupled and this calls for control strategies that are more complex than those for traditional two- or three-level converters. In particular, the submodules capacitors are difficult to balance as they are charged from the DC bus and discharged by the AC bus simultaneously. It is important to maintain the SM voltage ripple between boundaries for stability purpose; during unbalanced conditions this becomes an important challenge. Use of advanced control strategies to reduce the SM voltage ripple appears thus necessary.

Unbalanced fault condition is a common fault in grid-connected converters and during this condition both AC output current and the DC circulating current have to be controlled to their references (Yazdani and Iravani, 2006). In addition, the SM capacitor ripple has to be limited in order to avoid a parasitic trip of the converter on SM DC overvoltage condition. Most of the MMC control methods reported in literature consider a balanced operating condition and deal with balancing the capacitor voltages during transients. Pou *et al.* (2015) propose a SMs voltage ripple reduction method by injecting AC component in the circulating current, but three-phase unbalanced grid conditions are not considered. A circulating current controller of MMC based on components and able to operate under unbalanced conditions was proposed by Zhou *et al.* (2013) and Moon *et al.* (2013), but the consequences over the SMs voltage ripple are not analyzed in detail. Leon and Amodeo (2017) propose an energy-based control method that can improve the internal performance of MMC under unbalanced grid conditions, but this method contains many imbricated control loops whose tuning is quite difficult. The passivity-based control approach has also been recently proposed, that exploits the natural property of converters of storing and dissipating energy (Bergna *et al.*, 2015). Feedback-linearization-based control solutions relying upon average models have been proposed (Yang *et al.*, 2017); however, the intrinsic under-actuated nature of the dynamic system is difficult to handle.

This paper proposes a new control strategy based on a MIMO state-feedback control of both output (grid) and circulating current, whose tuning relies upon the balanced-grid model, but it is shown to also perform well during unbalanced conditions. This paper is organized as follows. Section 2 summarizes the balanced-grid three-phase MMC model, which is further used to design the proposed control strategy in Section 3. Section 4 discusses the numerical simulation results obtained on a comprehensive MATLAB®/Simulink® model. Conclusion is presented in Section 5, the final one.

2. MODELLING OF MMC UNDER BALANCED GRID AND CONVENTIONAL CONTROL

Figure 1 presents the configuration of a three-phase MMC, where submodule capacitors are denoted by *SM* and phases by *a*, *b* and *c*. Usual notations are introduced, namely: DC-link variables (current and voltage) are denoted by subscript "*d*", AC output variables by subscript "*s*", upper-arm variables are denoted by subscript "*u*" and lower-arm variables by subscript "*l*". *N* is the number of submodules in an arm, and *R* and *L* are the arm resistance and inductance, respectively. L_g is the grid inductance and $v_{ga,b,c}$ are grid voltages on each phase.

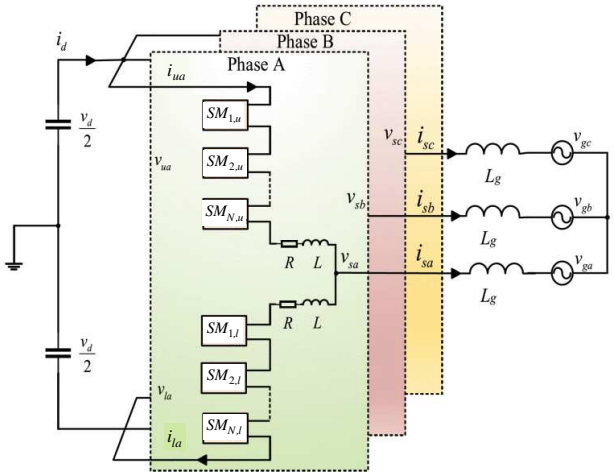

Fig. 1. Topology of a three-phase MMC, introducing notations of variables of interest.

On a single phase, for SM_i its voltage is noted $v^i_{cu,l}$ for upper/lower arm and its insertion index is defined as $n^i_{u,l}=1$ if SM_i is inserted and 0 otherwise. Voltage on an arm results as $v_{u,l}=\sum_{i=1}^{N} n^i_{u,l}\cdot v^i_{cu,l}$. Sum of capacitor voltages on an arm is defined as $v^{\Sigma}_{cu,l}=\sum_{i=1}^{N} v^i_{cu,l}$. Insertion index in an arm is defined as $n_{u,l}=(1/N)\sum_{i=1}^{N} n^i_{u,l}$. Supposing that all capacitor voltages are equal and combining the above expressions, one gets $v_{u,l}=n_{u,l}\cdot v^{\Sigma}_{cu,l}$. Output (grid) current i_s and output voltage v_s result as, respectively:

$$i_s=i_u-i_l\,,\ v_s=(v_l-v_u)/2 \tag{1}$$

Circulating current i_c and internal voltage v_c are defined as:

$$i_c=(i_u+i_l)/2\,,\ v_c=(v_l+v_u)/2 \tag{2}$$

Ideally, $i_c=i_u=i_l=i_d/3$ and $v_c\approx v_d/2$. v_s is sinusoidal between $v^{\Sigma}_{cl}/2$ and $-v^{\Sigma}_{cu}/2$. Conventional control of circulating current i_c and output current i_s is based on their dynamic equations:

$$\begin{cases}\dot{i}_c=-R/L\cdot i_c-1/(2L)\cdot v_u-1/(2L)\cdot v_l+1/(2L)\cdot v_d\\ \dot{i}_s=-R/L\cdot i_s-1/L\cdot v_u+1/L\cdot v_l-2/L\cdot v_a\end{cases} \tag{3}$$

By replacing v_s from (1) and v_c from (2) into (3), one obtains that i_c obeys a first-order DC-circuit dynamic and i_s respects a first-order AC-circuit dynamic:

$$\dot{i}_c=-R/L\cdot i_c-v_c/L+1/(2L)\cdot v_d \tag{4}$$

$$\dot{i}_s=-R/L\cdot i_s+2/L\cdot v_s-2/L\cdot v_a \tag{5}$$

By taking v_c in (4) and v_s in (5) as control inputs, the two currents can be separately controlled by using proportional-integral (PI) and proportional-resonant (PR) linear controllers (Sharifabadi *et al.*, 2016). Thus, i_c must be kept at a constant reference, meanwhile rejecting its double-grid-frequency (2ω) ripple, and i_s must track a grid-frequency (ω) sinusoidal reference.

Conventional control also comprises an upper-level, slower arm energy controller. Energy accumulated in the upper/lower arm's capacitors is noted by $W_{u,l}$. Energy sum is defined as $W_{\Sigma}=W_u+W_l$ and energy difference is $W_{\Delta}=W_u-W_l$. W_{Σ} obeys a DC-circuit dynamic and must be controlled at $W_{\Sigma 0}=C\cdot v_d^2/N$, while W_{Δ} is controlled in AC at 0. To this end, i_c is used as control input, with two components: a DC one to control W_{Σ} and an AC one to control W_{Δ}. These slower control loops thus provide Δi_c^*:

$$\Delta i_c^*=K_{\Sigma}\cdot\left(W_{\Sigma 0}-LPF\{W_{\Sigma}\}\right)-K_{\Delta}\cdot LPF\{W_{\Delta}\}\cdot cos(\omega t)\,, \tag{6}$$

with $LPF\{\cdot\}$ standing for low-pass filtering. Δi_c^* contributes to forming reference i_c^* for the lower-level, faster i_c control loop based on (4) (Sharifabadi *et al.*, 2016). Gains K_{Σ} and K_{Δ} are selected to ensure desired bandwidths.

3. STATE-FEEDBACK CONTROL DESIGN

The new control design resumes the state equations (4) and (5) characterizing the dynamics of the two currents on a single phase. Note that these dynamics are coupled at the input level: upper- and lower-arm voltages, v_u and v_l, respectively, intervene in both, they will be now the control inputs. The DC voltage v_d acts as a constant disturbance on the second-order system (1), while voltage v_a is perceived as a grid-frequency sinusoidal disturbance. Note that v_d also contains a double-grid-frequency ripple.

$$\begin{cases}\dot{i}_c=-R/L\cdot i_c-1/(2L)\cdot v_u-1/(2L)\cdot v_l+1/(2L)\cdot v_d\\ \dot{i}_s=-R/L\cdot i_s-1/L\cdot v_u+1/L\cdot v_l-2/L\cdot v_a\end{cases} \tag{7}$$

A full-state feedback can be designed for the MIMO plant (7) in order to place a desired closed-loop dynamics and also to ensure a constant-reference tracking for the DC-component of i_c, an ω-sinusoidal-reference tracking for i_s, as well as a 2ω-sinusoidal disturbance rejection on i_c. To ensure zero-steady-state-error reference tracking and disturbance rejection, five additional integral states are defined:

$$\begin{cases} \dot{x}_{i1} = -x_{i2} + i_s^* - i_s \\ \dot{x}_{i2} = \omega^2 \cdot x_{i1} \end{cases} \quad \dot{x}_{i3} = i_c^* - i_c \quad \begin{cases} \dot{x}_{i4} = -x_{i5} + i_c^* - i_c \\ \dot{x}_{i5} = 4\omega^2 \cdot x_{i4} \end{cases}$$

where *-notations denote references. That is, states x_{i1} and x_{i2} correspond to a resonant integrator on ω, state x_{i3} is that of an ordinary integrator and, finally, states x_{i4} and x_{i5} belong to a resonant integrator on 2ω. A MIMO extended plant with $\mathbf{x}_e = [i_c \quad i_s \quad x_{i1} \quad x_{i2} \quad x_{i3} \quad x_{i4} \quad x_{i5}]^T$ as states, $\mathbf{u}_e = [v_u \quad v_l]^T$ as vector control input and $\mathbf{u}_p = [v_d \quad v_a]^T$ as disturbance input is thus obtained; it is described by the state-space equation $\dot{\mathbf{x}}_e = \mathbf{A}_e \cdot \mathbf{x}_e + \mathbf{B}_e \cdot \mathbf{u}_e + \mathbf{B}_p \cdot \mathbf{u}_p$, where state matrix $\mathbf{A}_e$ and input matrices $\mathbf{B}_e$ and $\mathbf{B}_p$ are as follows:

$$\mathbf{A}_e = \begin{bmatrix} -R/L & 0 & 0 & 0 & 0 & 0 & 0 \\ 0 & -R/L & 0 & 0 & 0 & 0 & 0 \\ 0 & -1 & 0 & -1 & 0 & 0 & 0 \\ 0 & 0 & \omega^2 & 0 & 0 & 0 & 0 \\ -1 & 0 & 0 & 0 & 0 & 0 & 0 \\ -1 & 0 & 0 & 0 & 0 & 0 & -1 \\ 0 & 0 & 0 & 0 & 0 & 4\omega^2 & 0 \end{bmatrix}$$

$$\mathbf{B}_e = \begin{bmatrix} -1/(2L) & -1/L & 0 & 0 & 0 & 0 & 0 \\ -1/(2L) & 1/L & 0 & 0 & 0 & 0 & 0 \end{bmatrix}^T$$

$$\mathbf{B}_p = \begin{bmatrix} 1/(2L) & 0 & 0 & 0 & 0 & 0 & 0 \\ 0 & -2/L & 0 & 0 & 0 & 0 & 0 \end{bmatrix}^T$$

After checking controllability of matrix pair ($\mathbf{A}_e$, $\mathbf{B}_e$), a full-state feedback control of form $\mathbf{u}_e = -\mathbf{K}_e \cdot \mathbf{x}_e$ can be computed such as the closed-loop system $\dot{\mathbf{x}}_e = (\mathbf{A}_e - \mathbf{B}_e \cdot \mathbf{K}_e) \cdot \mathbf{x}_e$ to have a desired seven-order dynamics (Sobel *et al.*, 2011). To this end, two of the new poles correspond to render faster the original second-order dynamic of the two currents, i_c and i_s, by imposing that grid current i_s behaves faster than i_c in closed loop. Indeed, such a requirement corresponds to the necessity that AC power exchange to be faster than evolution of internal variables. The other remaining five poles – corresponding to the integral states – should be placed sufficiently far away (at least a decade) in relation to the accelerated second-order dynamic of the two currents, such as to not become dominant, as their role is to ensure zero steady-state error. Vector control input is $\mathbf{u}_e = [v_u^* \quad v_l^*]$. Internal voltage $v_c^* = (v_u^* + v_l^*)/2$ and grid voltage $v_s^* = (v_l^* - v_u^*)/2$ are further computed. *-notation is used because these variables are send as references to the modulation process, in order to obtain the desired upper- and lower-arm insertion indices, $n_u^* = (v_c^* - v_s^*)/v_{cu}^{\Sigma}$ and $n_l^* = (v_c^* + v_s^*)/v_{cl}^{\Sigma}$, respectively. Figure 2 shows the extended system's poles placement in relation to the original second-order dynamic for the three-phase MMC whose parameters are given in the Appendix. Thus, i_s closed-loop dynamic is imposed to be five times faster than the original one, while i_c closed-loop dynamic remains the same as in open loop. Dynamics of integral states are placed at much higher frequencies. The open-loop and imposed closed-loop poles, as well as the resulted gain $\mathbf{K}_e$ are given in the Appendix.

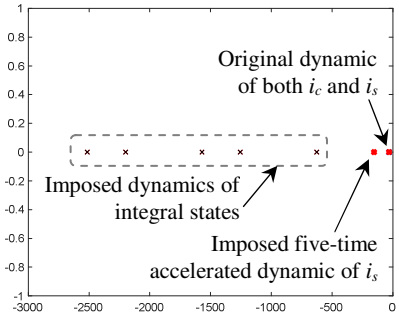

Fig. 2. Open-loop *vs.* imposed closed-loop dynamics.

The three-phase block diagram of the proposed control is given in Fig. 3, where three-phase variables are involved. Vector gain $\mathbf{K}_{e\_3phase}$ is the three-phase extension of single-phase gain $\mathbf{K}_e$. Note that, as an external reference cannot be imposed for the circulating current, another solution is achieved in practice. This consists in generating i_c^* based on low-pass filtering the measured current, i_c (Sharifabadi *et al.*, 2016), as the prevailing goal is to smooth i_c.

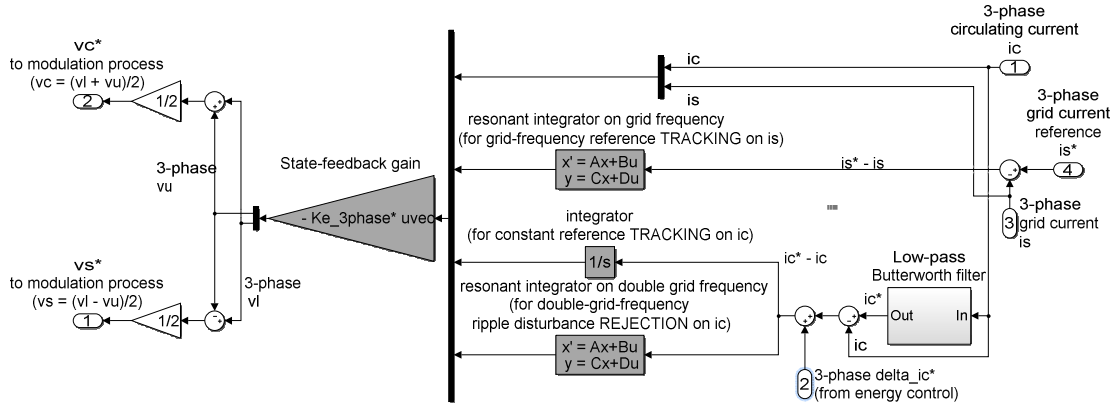

Fig. 3. Three-phase block-diagram implementation of the proposed MIMO full-state feedback control.

Note also presence of a component Δi_c^* coming from the energy control loop according to (6) and added to result in the final circulating current reference.

4. NUMERICAL SIMULATION RESULTS

The proposed control strategy is validated on a comprehensive MATLAB®/Simulink® model of a three-phase MMC, whose parameters are given in Appendix A. A comparison with the conventional control solution, habitually implemented in practice and based on multiple cascaded control levels (Sharifabadi *et al.*, 2016), is here discussed. Namely, the global multiple-level-based control approach is here preserved, with the difference that the proposed state-feedback controller replaces the two separate control loops of i_c and i_s. Thus, energy control level, as well as capacitor voltage balancing and modulation implementation, is left in place, aiming at showing that improved performance can be achieved with little adaptation effort.

A scenario of 1.3 seconds is chosen for illustration, with an unbalance in the grid conditions occurring at time 0.7 s and ending at time 1.1 s. While balanced grid is characterized by grid voltage positive sequence v_{g_pos} = 1 p.u. and by grid voltage negative sequence v_{g_neg} = 0 p.u., an unbalance in the grid is indicated by values different from these ones. Here, the unbalance is characterized by v_{g_pos} = 0.8 p.u. and v_{g_neg} = 0.2 p.u.

Figure 4 shows the internal control results when conventional control of i_c and i_s is in place. In this case, two separate loops are respectively in charge with controlling the two currents. Note that the control is no longer effective once the voltage unbalance takes place. As a consequence, increasing-magnitude oscillations in both three-phase circulating current (second plot) and sum of capacitor voltages, $v_{cu,l}^{\Sigma}$, (first plot) can be noted. For these latter, overpassing 10% of the rated value may result in MMC decoupling to avoid capacitors damage. Control of energy sum W_{Σ} (third plot) is slow and exhibits a quite important steady-state error. Energy difference W_{Δ} control has quite large variations from zero, its reference.

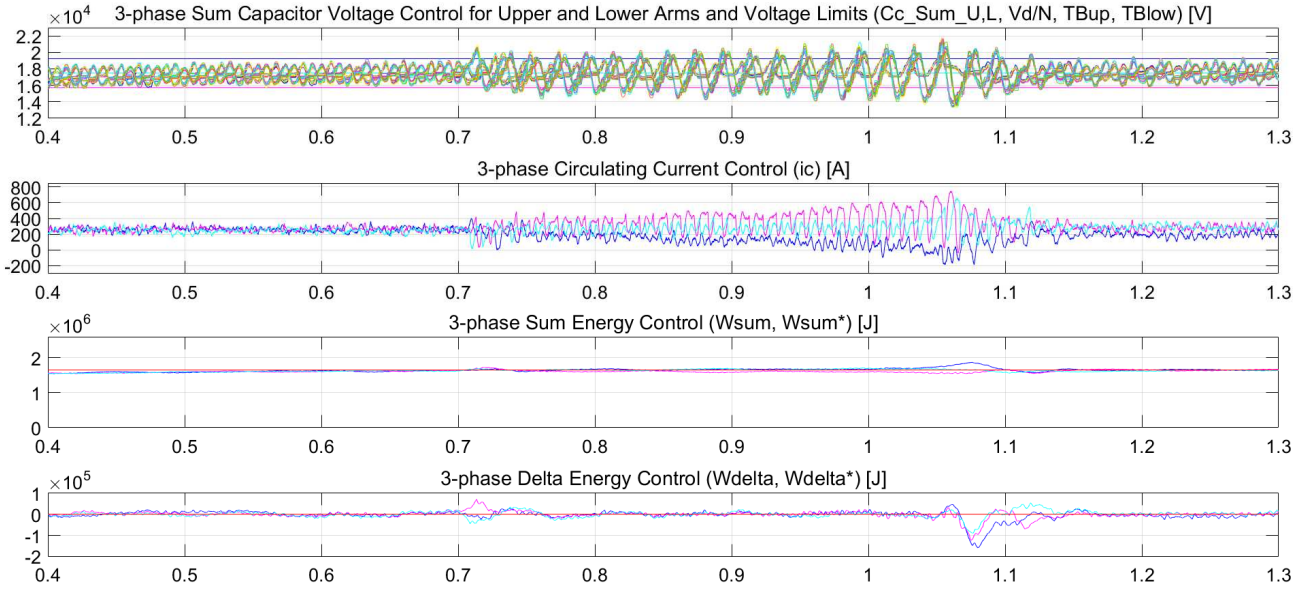

Fig. 4. Numerical simulation results obtained for the *conventional internal* control, based on separate loops for i_c and i_s, under unbalanced grid conditions occurring at time 0.7 s and lasting 0.4 s (v_{g_pos} = 0.8 p.u. and v_{g_neg} = 0.2 p.u.).

Results of internal control by state feedback are presented in Figure 5, where evolutions of the same variables as in Figure 4 can be seen. Circulating current i_c and output grid current i_s are now controlled according to the block diagram in Figure 3. Note that the closed-loop behaviour is no longer oscillating once the voltage unbalance takes place. Circulating currents on two of the phases stabilize at quite the same values, while on the third phase the i_c steady-state value is larger. Control of energy sum W_{Σ} is here faster – with some overshoot at transients between normal and unbalanced grid, and inversely – and has reduced steady-state error, while the energy difference is well maintained around zero.

Figure 6 shows the grid control results when conventional control of i_c and i_s is in place. Occurrence of the grid voltage unbalance can clearly be identified on the first plot. The second and the third plot present the closed-loop performance of d and q components of output current positive and negative sequence, respectively. The fourth plot displays active and reactive power evolutions, where oscillating behaviours can be noted during the grid fault.

Figure 7 shows the grid control results when state-feedback control of i_c and i_s is in place. One can note that the proposed control results in an improvement of positive and negative sequences of grid current control, in terms of both precision and transients between faulted and normal grid conditions (second and third plot, respectively), which positively impacts power evolution (fourth plot).

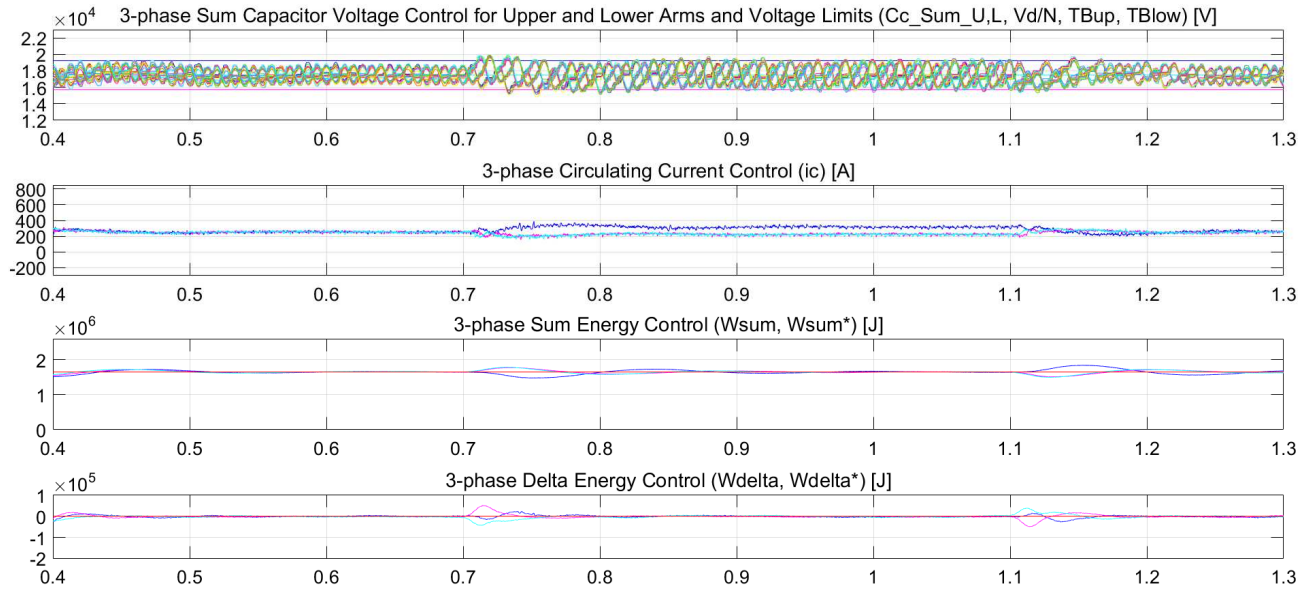

Fig. 5. Numerical simulation results obtained for the MIMO *state-feedback internal* control of both i_c and i_s, under unbalanced grid conditions occurring at time 0.7 s and lasting 0.4 s (v_{g_pos} = 0.8 p.u. and v_{g_neg} = 0.2 p.u.).

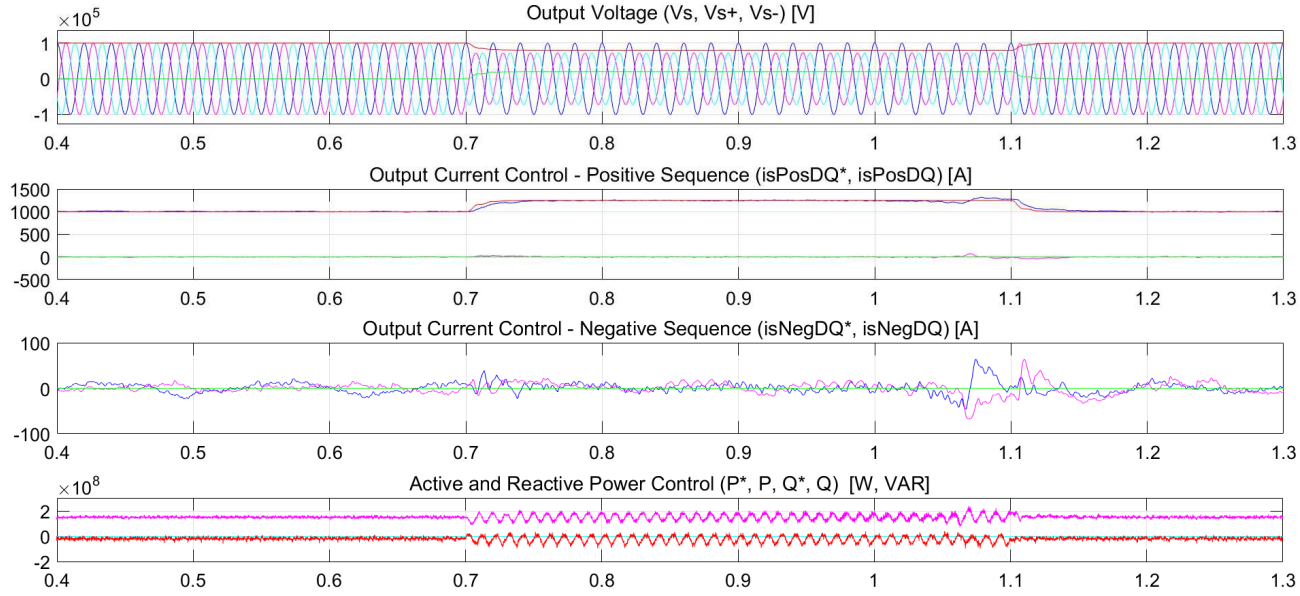

Fig. 6. Numerical simulation results obtained for the *grid variables* control when i_c and i_s are controlled by separate loops, under unbalanced grid conditions occurring at time 0.7 s and lasting 0.4 s (v_{g_pos} = 0.8 p.u. and v_{g_neg} = 0.2 p.u.).

5. CONCLUSION

A MIMO state-feedback control of both grid and circulating current in MMCs has been proposed, which allows that the input-coupled dynamics of the two currents to be controlled together. Thus, imposing desired closed-loop reference tracking and disturbance rejection dynamics of the two currents is stated as a MIMO pole-placement problem. The design procedure is detailed and the strategy is validated on a comprehensive MATLAB®/Simulink® model of a three-phase MMC. Under unbalanced grid conditions, simulation results show improved performance against the conventional control featuring two separate control loops**.** The proposed control method shows a good stability and accurate control of DC circulating current during the *unbalanced*-grid fault, still remaining based on the *balanced*-grid model of MMC. The submodule capacitor voltage ripple is thus maintained within admissible limits (±10% around rated) despite the fault, which is not the case for the conventional control. Control of grid currents is also improved. Well-performing internal control also allows reducing time response and precision of upper-level control loops, such as energy control. Future work will aim at confirming the numerical-simulation-proved effectiveness on a real MMC setup.

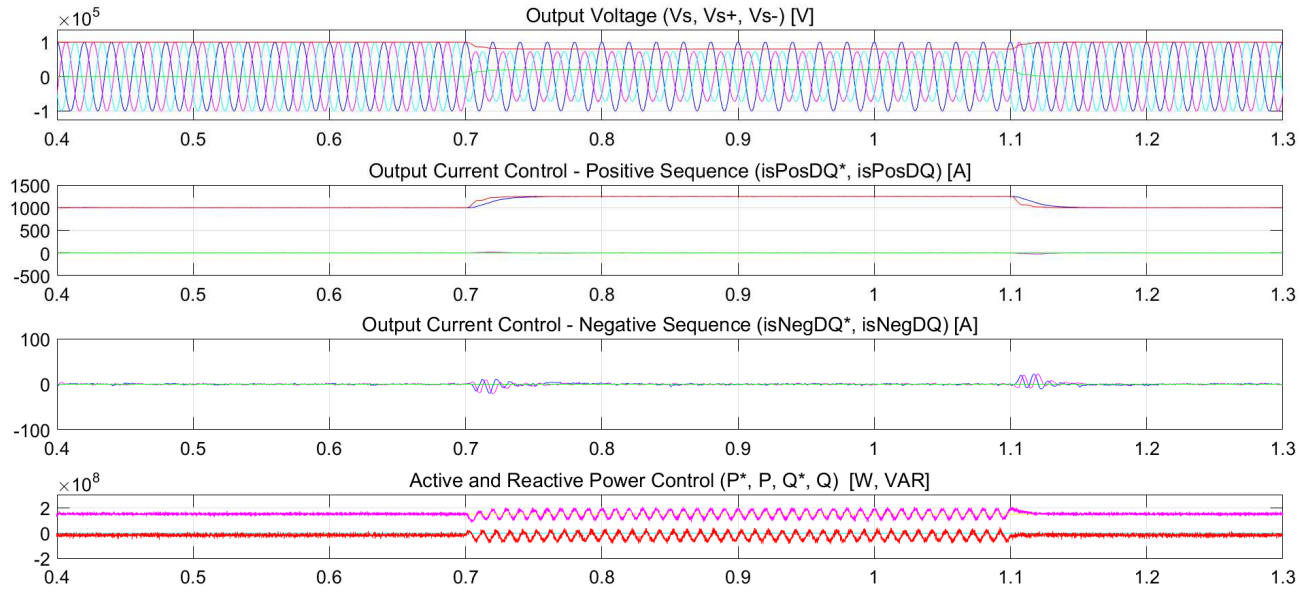

Fig. 7. Numerical simulation results obtained for the *grid variables* control when i_c and i_s are MIMO *state-feedback* controlled, under unbalanced grid conditions occurring at time 0.7 s and lasting 0.4 s (v_{g_pos} = 0.8 p.u. and v_{g_neg} = 0.2 p.u.).

REFERENCES

Bergna, G., Pirro, M., Berne, E., Arzandé, A., Molinas Cabrera, M., and Ortega, R. (2015). Modular Multilevel Converter Passivity-Based PI Control suited for Balanced and Unbalanced Grid Conditions. In: *Procs. of 2015 IEEE International Conference on Industrial Technology – ICIT 2015*, March 2015, Seville, Spain.

Leon, A.E., and Amodeo, S.J. (2017). Energy Balancing Improvement of Modular Multilevel Converters under Unbalanced Grid Conditions. *IEEE Transactions on Power Electronics*, 32(8), 6628-6637.

Marquardt, R., Lesnicar, A., and Hildinger, J. (2002). Modular converter concept for grid coupling application at high voltages (in German: Modulares Stromrichterkonzept für Netzkupplungsanwendung bei hohen Spannungen). In: *Proceedings of the ETG-Fachtagung*, 2002, Bad Nauheim, Germany.

Moon, J.W., Kim, C.S., Park, J.W., Kang, D.W., and Kim, J.M. (2013). Circulating current control in MMC under the unbalanced voltage. *IEEE Transactions on Power Delivery*, 28(3), 1952-1959.

Pou, J., Ceballos, S., Konstantinou, G., Agelidis, V. G., Picas, R., and Zaragoza, J. (2015). Circulating current injection methods based on instantaneous information for the modular multilevel converter. *IEEE Transactions on Industrial Electronics*, 62(2), 777-788.

Sharifabadi, K., Harnefors, L., Nee, H.-P., Norrga, S., and Teodorescu, R. (2016). *Design Control and Application of Modular Multilevel Converters for HVDC Transmission Systems*. John Wiley & Sons.

Sobel, K.M., Shapiro, E.Y., and Andry, A.N. (2011). Eigenstructure assignment. In (W.S. Levine, ed.) *The Control Handbook*, 2nd edition, pp. 16-1–16-20. CRC Press, Boca Raton, Florida, U.S.A.

Yang, S., Wang, P., and Tang, Y. (2017). Feedback Linearization Based Current Control Strategy for Modular Multilevel Converters. *IEEE Transactions on Power Electronics*, 33(1), 161–174.

Yazdani, A., and Iravani, R. (2006). A unified dynamic model and control for the voltage-sourced converter under unbalanced grid conditions. *IEEE Transactions on Power Delivery*, 21(3), 1620-1629.

Zhou, Y., Jiang, D., Guo, J., Hu, P., and Liang, Y. (2013). Analysis and control of modular multilevel converters under unbalanced conditions. *IEEE Transactions on Power Delivery*, 28(4), 1986-1995.

Appendix A. THREE-PHASE MMC PARAMETERS USED IN SIMULATION

Electrical parameters

Rated apparent power S_{rated}=150 MVA; DC-link voltage v_d=200 kV; output voltage amplitude V_{s_max}=100 kV; output current amplitude I_{s_max}=1 kA; grid frequency $\omega=2\cdot\pi\cdot50$ rad/s; number of submodules N=12; arm resistance R=1.6 Ω; arm inductance L=50.9 mH; submodule capacitance C=450 μF; grid resistance R_g=0.1 Ω; grid inductance L_g=3.2 mH; initial value of circulating current I_{c0}=250 A.

Open-loop poles: –31.4159, –31.4159 (rad/s)

Control parameters

Imposed closed-loop poles: –31.4159, –157.0796, –628.3185, –1570.8, –2199.1, –2513.3, –1256.6 (rad/s)

Full-state feedback control gain on each phase $\mathbf{K}_e$=

$$10^5 \cdot \begin{bmatrix} -0.0024 & -0.0018 & 1.6212 & 0.0004 & 0.0979 & 3.0020 & 0.001 \\ -0.0024 & -0.0018 & -1.6564 & -0.0004 & 0.1025 & 3.1648 & 0.0011 \end{bmatrix}$$

Arm energy controller gains on each phase: $K_\Sigma = 0.0005$, $K_\Delta = 0.001$.